In-situ Evaluation of the Polymer Concentration Distribution of Microphase Separated Polyelectrolyte Hydrogels by Microelectrode Technique

Takuya Nishimura[1], Honglei Guo[2,3], Ryuji Kiyama[1], Yoshinori Katsuyama[2], Jian Ping Gong[2,4] , Takayuki Kurokawa[*2]

[1] Graduate School of Life Science, Hokkaido University, Sapporo 001-0021, Japan

[2] Faculty of Advanced Life Science, Hokkaido University, Sapporo 060-0811, Japan

[3] School of Chemical Engineering and Technology, Sun Yat-sen University, ZhuHai, 519082, China

[4] Institute for Chemical Reaction Design and Discovery (WPI-ICReDD), Hokkaido University, Sapporo, 001-0021, Japan

* Corresponding author. Laboratory of Transformational Soft Matter, Faculty of Advanced Life Science, Hokkaido University, Sapporo, 001-0021, Japan. Tel: +81-11-706-9018

E-mail address: kurokawa@sci.hokudai.ac.jp

for Table of Contents use only

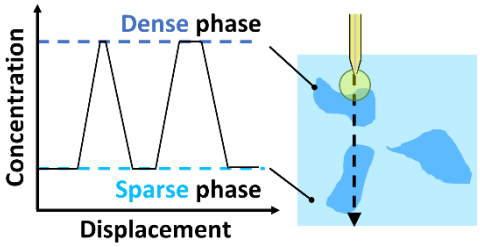

Abstract

The heterogeneous structure that exists in virtually all hydrogels has a significant influence on the resulting strength and toughness. While the internal structure has been observed with electron microscopy, it is difficult to measure the *in-situ* local polymer concentration in the native swollen state. In this study, a modified microelectrode technique (MET) was employed to measure the Donnan potential of a heterogeneous hydrogel with a phase separated structure. With this method we succeeded in observing quantitative, *in situ* polymer concentrations ranging from 10.2 micromole per liter to several hundred millimole per liter. From the obtained concentration profiles, we could successfully evaluate the internal phase separated structure with a resolution of less than 0.8 micrometers. Using MET, we could estimate the average activity coefficient of the hydrogel, and we found a difference in concentration between the dense and sparse phases. We demonstrate that MET is a powerful method that can locally and quantitatively measure the polyelectrolyte concentration distribution within hydrogels. Furthermore, this method can be applied to cells and organs *in vivo*, due to their similarities with polyelectrolytes. Enabling the *in-situ* determination of internal structures of biomaterials could have important implications towards characterization of damaged and diseased tissues on the local scale.

Introduction

Hydrogels consist of polymer networks that are highly swollen in water, resulting in various properties such as flexibility (low modulus), low friction, and biocompatibility.[1–3] Because of these properties, hydrogels are expected to be applied in various applications, such as replacing articular cartilage and industrial materials. However, a serious shortcoming of simple, single network hydrophilic hydrogels is that they are often weak and brittle. Developing methods to toughen hydrogels so that they can be used in real applications is an ongoing area of focus in the field. For example, polyelectrolytes are used in double network (DN) gels[4] because they can swell greatly in water, resulting in extended materials that are stiff and can break easily. This brittleness acts as a sacrificial bond, giving the DN gel its toughness. Also, in polyampholyte hydrogels[5] that are viscoelastic tough hydrogels, the charged structure directly results in phase separated structures that enable toughness. Thus, hydrogels consisting of electrolyte polymers and hydrogels with an internal phase separated structure have high mechanical properties and functions and are expected to be used in industrial applications. In particular, they are expected to be used, for example, as materials for innovative protectors[6], model materials for 3D printers, and actuators for soft robots.[7–11]

The internal microstructure of polyelectrolyte hydrogels can significantly impact the resulting physical properties of the gel, yet characterization is difficult. There are several methods to measure the spatial

heterogeneity inside hydrogels, including scattering techniques such as neutron scattering and light scattering[12-14], and imaging techniques such as confocal laser microscopy[15], scanning electron microscopy (SEM)[16] , and atomic force microscopy (AFM)[17]. Scattering methods can be used to characterize the sample-averaged structure and polymer concentration, which is molar concentration of fixed charges of the polyelectrolyte chains, but the local spatial arrangement cannot be determined. Microscopy can observe the local hydrogel structure but cannot provide quantitative information on the polymer concentration. Although SEM can observe the local morphology of the hydrogel surface, it requires processing such as freeze-drying, which inherently alters the hydrogel structure. AFM can also be used to observe the hydrogel surface *in situ*, but it does not provide information about the internal structure. The above methods each have their own advantages and disadvantages for *in-situ* observation of the local internal structure and quantitative polymer concentration of hydrogels, but no technique is able to acquire all of this information simultaneously.

We propose the microelectrode technique (MET) as a method for in-situ observation of heterogeneity in hydrogels. MET has been widely used in biology to measure nerve action potentials.[17–22] MET has also been used to characterize synthetic hydrogels by measuring the Donnan potential inside of polyelectrolyte hydrogels, which allowed us to study the difference in the density of polyelectrolytes

due to the differences in swelling of the hydrogel. MET can be applied to hydrogels that have immobile charges.[23–27]

The microelectrode method has been widely used in the past as a cell potential measurement technique. Recently, the microelectrode technique has been adapted to hydrogels, and a method to obtain the internal Donnan potential has been established. Safronov et al. successfully measured the time variation of the electric potential inside the hydrogel at a fixed point using a glass electrode with a diameter of 1 μm.[26] They clarified the relationship between the concentration of the external salt solution and the activity of the counterion in the hydrogel. Guo et al. set a glass electrode with a diameter of 150 nm in a manipulator to enable continuous measurement of electric potential in the depth direction of the gel.[24,27] They clarified the effect of the glass electrode on the fracture of the hydrogel surface and the internal fracture behavior of DN gels. In this study, we further improved the measurement method of Guo et al. and increased the spatial resolution of the instrument system by more than 30 times. This made it possible to follow the local potential, which changes according to the aggregation structure of the local network, with high accuracy. It also made it possible to evaluate the polymer concentration distribution from the locally obtained potential profile and the average activity coefficient of the hydrogel.

Polyelectrolyte hydrogels consist of charged groups covalently bound to the polymer backbone (fixed ions) and ions that can move in the aqueous solution (mobile ions). Among the mobile ions, those with the same charge as the fixed ions are called co-ions, and those with the opposite charge are called counterions. When there is a concentration difference between the inside of the gel and the outside solution, the mobile ions move across the gel-solution interface due to entropy. On the other hand, fixed ions attract counterions and repel co-ions by electrostatic interactions. Furthermore, this competition between electrostatic interaction and ion diffusion causes a concentration difference of counterions between the inside of the gel and the external solution, resulting in an electric double layer at the interface. Therefore, there is a potential difference, called the Donnan potential (Φ_D), between the reference solution and the polyelectrolyte gel.[28]

$$\Phi_D = \Phi_g - \Phi_s = \frac{2.3RT}{zF} log \frac{a_s}{a_g} = \frac{2.3RT}{zF} log \frac{\gamma_s C_s}{\gamma_g C_g} \quad (1)$$

Here, Φ is potential, a is activity, which is concentration of mobile counterions, γ is activity coefficient, z is the valence of the mobile ion in consideration, R is the gas constant, T is the absolute temperature, F is the Faraday constant, and C is the concentration of counterions. The subscripts g and s denote the parameters in the gel and in the solution, respectively.

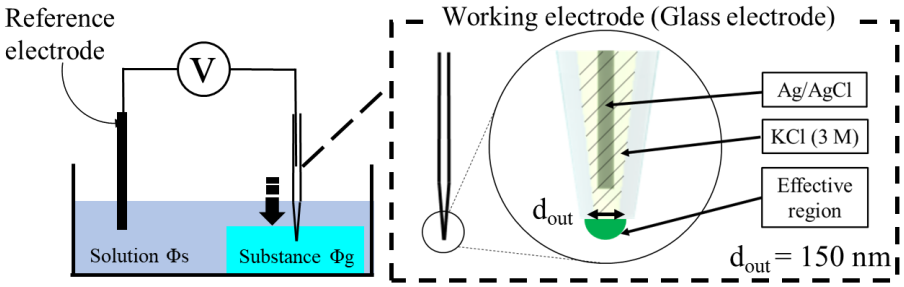

Figure 1. Schematic illustrations of the experimental setup for potential measurement. MET uses a voltmeter to measure the potential between a carbon electrode stationary in the reference solution and a glass electrode inserted into the measurement sample at a constant rate. The adapter that fixes the glass electrode is connected to the manipulator and can be continuously inserted into the measurement sample at a constant speed during the potential measurement. The glass electrode has a tip diameter of about 150 nm and contains 3 M KCl_{aq} and an Ag/AgCl wire.

An example of the testing setup used during MET experiments on a polyelectrolyte gel is shown in Figure 1. We measure the Donnan potential generated between a glass electrode inserted into the gel and a carbon electrode in the reference solution. 3 M KCl_{aq} and an Ag/AgCl wire are placed inside the glass electrode. The counterions corresponding to the fixed ions on the polymer chains undergo a redox reaction with the Ag/AgCl wire inside the glass electrode. The difference between the concentration of the counterions inside the gel and the ionic concentration in the reference solution is expressed as the Donnan potential. We constructed an improved experimental system that increases

the measurement quality and enables thorough noise removal. A carbon electrode is fixed in the reference solution, and a glass electrode with a tip diameter of about 150 nm is inserted perpendicular to the gel at a constant speed (0.8 μm/sec) to measure the electric potential, which enables us to measure the potential of the local area spatially and continuously.

Since we observe on a scale (μm scale) that is sufficiently larger than the mesh size of the hydrogel (nm scale), the potential obtained by MET reflects the average value of the counterion concentration within the measurement range of the glass electrode tip. Also, this measurement range is sufficiently larger than the Debye length of the counterions around the fixed ion on the polyelectrolyte chain. Therefore, the charge of the polyelectrolyte chain and the counterions maintain electrical neutrality, and the average counterions concentration over a volume of the probe is considered to be equal to the charge density of the electrolyte polymer chain or polymer concentration. Therefore, if the MET is applied to hydrogels, it is possible to obtain a continuous potential distribution in the direction of travel. From the potential distribution, it is possible to characterize the sparse and dense structure of a polyelectrolyte due to differences in the network density and the polymer concentration distribution. When the ion concentration in the bath solution is much lower than the concentration of immobile ions of the gel, the co-ion concentration inside the gel is negligibly low, and the counterions concentration

calculated from the Donnan potential is equivalent to the immobile polyelectrolyte concentration, from the electric neutrality condition.

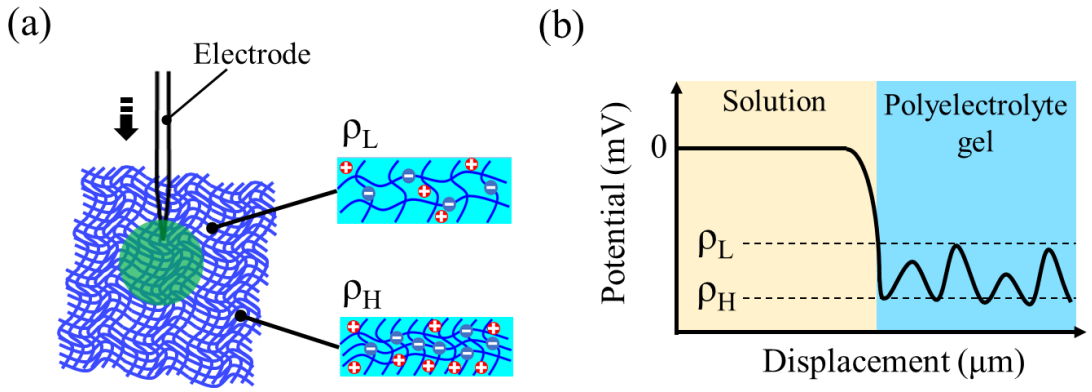

Figure 2. Relationship between Donnan potential and density of polyelectrolyte chain density. (a) Schematic image of the local polyelectrolyte density and the detection range of the glass electrode. ρ is the network density of polyelectrolyte chains. The higher the polymer chain density, the higher the concentration of counterions trapped in the polymer chain, and the larger the absolute value of the potential. (b) Illustration of a potential profile of a negatively charged hydrogel. The potential profile is shown with potential (mV) on the vertical axis and displacement (μm) on the horizontal axis. A glass electrode is inserted at an arbitrary position in the reference solution and used as a reference for potential 0. The potential decreases rapidly around the point where the glass electrode contacts the gel, and the potential fluctuates inside the gel.

Next, we consider how the heterogeneous network structure is expressed in the potential profile. A polyelectrolyte gel consisting of negatively charged polymer chains containing both sparse and dense internal regions, as shown in Figure 2(a), is considered as a model. When the gel is measured by the MET, the expected potential profile is shown in Figure 2(b). The potential profile obtained by the MET is represented by displacement (unit: μm, the distance the glass electrode has moved) on the horizontal axis and potential (unit: mV, the local potential of the hydrogel) on the vertical axis. The potential when the glass electrode is located in the reference solution is 0 mV. When the glass electrode touches the electrolyte hydrogel with a negative charge, the potential will change significantly in the negative direction. Here, the larger the density (ρ) of the polymer chain, the higher the counterion concentration of the fixed ions on the polymer chain, and the larger the absolute value of the potential. An illustration of the potential profile of the continuously measured Donnan potential inside the heterogeneous hydrogel is shown in Figure 2(b). The potential change can reflect the sparse and dense structure of the network of the heterogeneous electrolyte hydrogel and the polymer concentration change.

In this study, we use the microelectrode technique to evaluate the internal structure of hydrogels with internal heterogeneity and measure the polymer concentration distribution quantitatively. As a hydrogel model with heterogeneity, a hydrogel with an internally phase separated sea-island structure

(referred to as a phase separated gel) is used. The gel was synthesized by using a dioxane/water mixed solvent in the precursor monomer solution of the gel. Since dioxane is a poor solvent for the polymer, it is possible to create a polyelectrolyte hydrogel with a micron-scale non-uniform phase separated structure consisting of a dense phase and a sparse phase.[29] We can adjust the degree of internal phase separation of this gel by varying the fraction of dioxane in the mixture solvent. As a result, we find that the quantitative concentration of aggregates inside the phase separated hydrogel and their spatial distribution could be successfully evaluated with sub-micron scale resolution using MET. Using MET, we propose a new index, the polyelectrolyte density distribution for designing highly functional hydrogels with toughness and viscoelasticity. Furthermore, in the future MET can be applied to cells and organs *in vivo*, due to their similarities with polyelectrolytes. Enabling the *in-situ* determination of internal structures of biomaterials could have important implications towards characterization of damaged and diseased tissues on the local scale.

Experimental

・Materials

2-Acrylamido-2-methylpropanesulfonic acid sodium salt (NaAMPS) was provided courtesy of Toa Gosei Co., Ltd. Dimethylacrylamide (DMAAm), N, N′ -Methylenebis(acrylamide) (MBAA), 2-oxoglutaric acid (OA), potassium chloride (KCl), sodium chloride (NaCl), iron (Ⅲ) chloride hexahydrate, iron (Ⅱ) chloride tetrahydrate and 1,4-dioxane were purchased from FUJIFILM Wako Pure Chemical Industries, Ltd. All materials were used as received.

・Synthesis of phase separated single network gels[29]

We prepared hydrogels with dioxane, resulting in an internally phase separated structure. Dioxane is a poor solvent for poly(NaAMPS) while NaAMPS monomers are soluble in dioxane. Therefore, when the monomer is dissolved in a mixture of dioxane and water and polymerized, the polymer aggregates during polymerization.

Negatively charged monomer (NaAMPS: 1 M), cross-linker (MBAA : 3 mol% relative to NaAMPS concentration), and initiator (OA: 0.1 mol% relatives to NaAMPS concentration) were dissolved in a mixed solvent. The dioxane weight fractions (r) of mixed solvents were 0, 0.1, 0.2, 0.3, 0.4, 0.5, and 0.54. We poured the solution into a glass mold consisting of two soda-lime glass plates (thickness = 3

mm) separated by a U-shaped silicone rubber sheet (thickness = 2 mm). The mold was irradiated with UV light (365 nm; 4 mW / cm^2) for 9 hours. The prepared hydrogels were immersed in deionized water, and the immersion water was changed daily for about two weeks to remove dioxane, residual monomers, and initiators. The degree of removal of residual monomers and other substances was checked using a conductivity meter. Gas chromatography (GC-2014, SHIMADZU, Japan) was used to check the residual dioxane concentration in the washing solution.

・Synthesis of the phase separated DN gel

The phase separated single network gels after the removal of residues were very brittle and unsuitable for MET measurements. Therefore, we increased the toughness of the phase separated gel by employing the double network concept. Neutral monomers were used as the reinforcing network as to not affect the MET measurement. The phase separated gels were immersed in an aqueous solution of a neutral monomer (DMAAm: 2 M), cross-linker (MBAA: 0.1 mol% of DMAAm concentration), and initiator (OA: 0.1 mol% of DMAAm concentration) for two days. After immersion, the poly(NaAMPS) gel was sandwiched between two soda-lime glass plates. The gels were then irradiated with UV light (365 nm; 4 mW/cm^2) for 9 h under Ar atmosphere. The prepared hydrogels were immersed in deionized water, and the soaking water was changed daily for about one month to remove

residual monomer and initiator. After that, the phase separated DN gel swollen to 3-5 mm in thickness was immersed in 10^{-5} M $NaCl_{aq}$ for more than two days to reach equilibrium.

・Preparation of glass electrodes

The glass electrodes were made by stretching a glass tube (BF100-75-15, Sutter, USA) using a Puller (P-2000, Sutter, USA). The diameter of the glass tube was 0.78 mm, and the total length was about 7.5 cm. The tip length and diameter of the glass electrodes varied depending on various parameters such as stretching speed, stretching force, and stretching time. The electrical resistance in the reference solution also varies with these parameters. In this system, glass electrodes with a tip diameter of about 150 nm, a resistance value of 20-60 MΩ, and a vertically aligned diameter were prepared.

・Potential measurement of the phase separated DN gel

A glass electrode controlled by a micromanipulator (DMA-1511, Narishige, Japan) was inserted into the phase separated DN gel from an external reference solution at a constant speed. The glass electrode tip diameter used in this study was 150 nm, and the reference solution was 10^{-5} M $NaCl_{aq}$.

・Imaging of the phase separated DN gel by TEM[30]

To stain the polyelectrolyte, we mineralized Fe particles in the poly(NaAMPS) network of a phase separated DN gel. The staining solutions used were 2.5 M $FeCl_3$ and 1.5 M $FeCl_2$. Amorphous iron oxide nanoparticles were grown on the poly(NaAMPS) network by immersing the gel containing Fe ions in pure water to increase the pH. We then froze the phase separated DN gels in liquid nitrogen. The water in the phase separated DN gels was replaced by acrylic resin (London Resin white, medium) using an automated freeze-substitution system (EM AFS2, Leica Microsystems, Germany) and then cut into 100 nm sections. The sections were observed by transmission electron microscopy (TEM, H-7650, Hitachi, Japan). The acceleration voltage of the electron gun for observation was set at 100 kV.

Result and Discussion

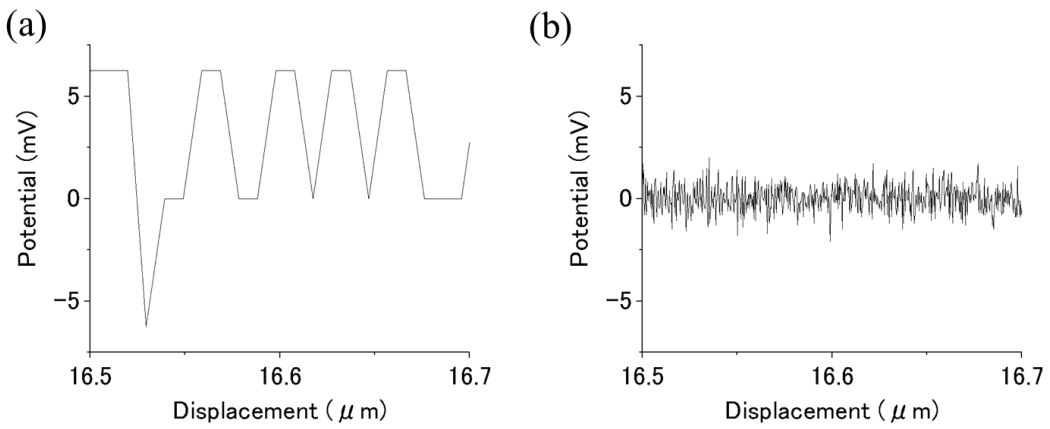

Figure 3. The potential fluctuation and noise in the reference solution reported in a previous study compared to the results obtained in the current work. (a) The profile obtained by the previous method with an older oscilloscope: the potential resolution was 6.25 mV, and the spatial resolution was 9.9×10^{-3} μm. (Conditions: potential full scale, ±1.5 V; A/D conversion, 8 bit; sampling rate, 200 /s; insert speed, 2.0 μm/s). (b) The profile obtained in this work with the new oscilloscope: the potential resolution is 0.1 mV, and the spatial resolution is 3.2×10^{-4} μm. (Conditions: potential full scale, ±5 V; A/D conversion, 12 bit; sampling rate, 2500 /s; insert speed, 0.8 μm/s). Reference solution was 10^{-5} M $NaCl_{aq}$.

The measurement system used in the previous study had a large noise level, and the resolution of the measurement equipment did not keep up with the resolution of the microelectrode technique.[18]

Therefore, we updated the measurement system to measure the local potential of the polyelectrolyte hydrogel more precisely. First, we replaced the oscilloscope with a 12-bit A/D convertor (TELEDYNE LECROY, HDO6034, USA). Next, we performed noise treatment around the wiring. Specifically, ferrite cores (TDK, ZCAT2035-0930A-BK, Japan) were attached to the power cables of each device, and wire mesh shields (MiSUMi, FLS-12-10, Japan) were placed on the outside of the signal cables. We also used a power supply with a ground noise filter (SANWA supply, TAP-3811NFN, Japan).

The potential profile in the reference solution of the previous oscilloscope (Iwatsu, DS-4264, Japan) is shown in Figure 3(a), and the potential profile obtained from the new oscilloscope is shown in Figure 3(b). The full scale of the potential profile in Figure 3(a) measured by the previous oscilloscope was ±1.5 V, the A/D conversion was 8 bits, the sampling rate was 200 /s, and the insertion speed of the glass electrode was 2.0 μm/s. Analysis of these results show that the potential resolution of the previous oscilloscope was 6.25 mV, the spatial resolution was 9.9×10^{-3} μm, and the standard deviation of the white noise was ± 3.8 mV. The full scale of the potential profile in Figure 3(b) measured by the new oscilloscope was ± 5 V, the A/D conversion was 12 bits, the sampling rate was 2.5 K /s, and the insertion speed of the glass electrode was 0.8 μm/s. In contrast to the previous oscilloscope, the new system showed the resolution of the potential of the new oscilloscope was 0.1 mV, the spatial resolution was 3.2×10^{-4} μm/S, and the standard deviation of the white noise is ± 0.63 mV. These

improvements increased the effective number of samples by a factor of about 38 and allowed us to obtain a spatial resolution of the device sufficient to detect local potential changes. Also, we reduced the white noise level to about 1/6. With this reduction, we found that we could detect concentration changes of more than 1.02×10^{-5} M (2%) in a 10^{-5} M NaCl solution. It was also assumed that the standard deviation of the white noise does not change regardless of the value of the potential.

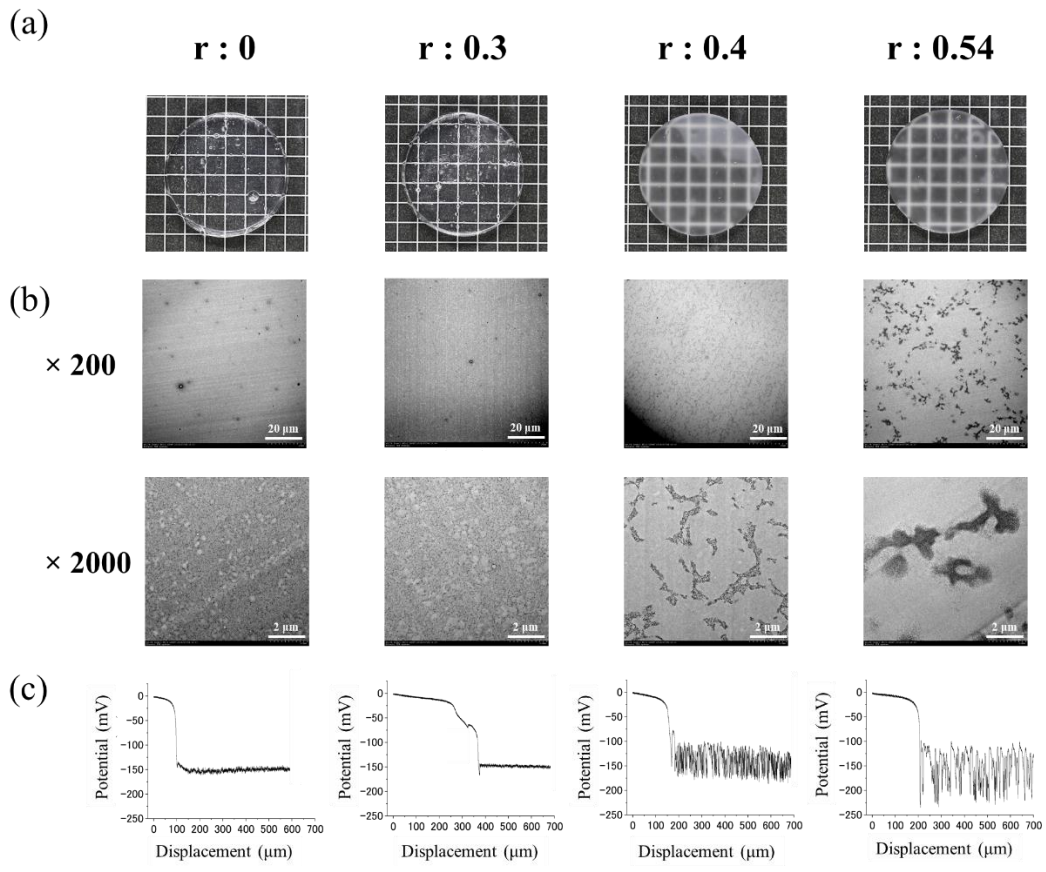

Figure 4. TEM and MET evaluation of phase separated DN gels prepared in dioxane/water mixture solvents of various dioxane weight fraction, r. (a) Photographs of the phase separated DN gels after

swelling. (b) TEM images of the phase separated DN gels at different magnifications. (c) Potential profiles of phase separated DN gels measured by MET.

The gel samples used for the Donnan potential and TEM measurements were each cut out from a single gel sheet. We will compare the optical clarity of gels and their microscopic structure with changing dioxane content during synthesis. As shown in Figure 4(a), the gel was transparent when the dioxane weight fraction was $r \leq 0.3$, while it became cloudy when $r \geq 0.4$. We confirmed this by TEM images and measured the inside of the phase separated DN gel by MET measurements for r = 0, 0.3, 0.4, and 0.54. The poly(NaAMPS) chains of the phase separated DN gels were stained by Fe mineralization and observed by TEM in Figure 4(b). These TEM images showed that there was no aggregation of the poly(NaAMPS) chains with dioxane weight fractions from 0 and 0.3. Furthermore, increasing the dioxane concentration to r = 0.4, phase separation occurred, resulting in a dense phase with a higher concentration of poly(NaAMPS) chains and a sparse phase with a lower concentration of poly(NaAMPS) chains, with an average dense phase size of 2.0 ± 0.6 μm at r = 0.4 and a dense phase with high contrast at r = 0.54. Here, the size of the dense phase is expressed as mean ± the standard deviation (Number of samples: 50). Also, according to the discussion by Kiyama et al.[30], the thickness of the DN gel shrinks by about 15% in length during the TEM sample preparation process.

Therefore, the size of the dense phase obtained by TEM observation is the size of the gel after shrinkage. Assuming the same shrinkage rate for this phase separated DN gel, and correcting for the shrinkage, the size of the dense phase is 2.4 ± 0.7 μm for r = 0.4 and 5.2 ± 1.2 μm for r = 0.54 respectively.

The dense phase that contains a higher content of poly(NaAMPS) chains has more negative charge, and the resulting potential is larger in the negative direction. From this point on, the absolute value of the potential is used when comparing the magnitude of the potential. The results of MET were shown in Figure 4(c). The fluctuation of the potential profile was slight for r = 0 to 0.3. In contrast, the fluctuation of the potential profile from r=0.4 to 0.54 was more significant. Considering that the potential is larger in the dense phase and smaller in the sparse phase, the potential band of about -100 mV represents the sparse polyelectrolyte phase, and the potential band of about -200 mV represents the dense polyelectrolyte phase. This trend of potential fluctuation was consistent with the presence or absence of phase separated structures in the gel photographs and TEM images. MET possesses sufficient resolution that we can clearly measure potential changes that are related to the local structure.

Next, we calculated the polymer concentration, which is molar concentration of fixed charge of poly(NaAMPS) inside the hydrogel from the obtained potential profile. As mentioned in the previous

discussion, the polymer concentration and counterions concentration (C_g) are considered to correspond 1:1 because the charges of the polyelectrolyte chains and counterions are electrically neutral in this experimental system. Therefore, we calculated the counterion concentration (C_g) around the polyelectrolyte chain inside the gel according to equation (1), which can be re-written for simplicity as

$$C_g = \frac{C_s \gamma_s}{10^{\frac{zF\Phi_D}{2.3RT}}} \times \frac{1}{\gamma_g} = \frac{a_g}{\gamma_g} \quad (2)$$

In this study, 10^{-5} M NaCl solution was used as the reference solution, so $C_s = 10^{-5}$ and z = 1. The activity coefficients of ions in the NaCl solution with such a low concentration could be considered as an ideal solution, so we assumed $\gamma_s \approx 1$. Here, the activity coefficient of the mobile counterions (γ_g) should change with the polymer concentration in the phase separated structure. It was assumed that the activity coefficient in the concentrated phase of the phase separated DN gel decreases because the relative dielectric constant around the polymer chains decreases, and the activity coefficient also decreases.[21] Conversely, the activity coefficient in the sparse phase was assumed to be larger. The method to measure the activity coefficient in the dense phase and the sparse phase has not yet been established. Therefore, we calculated the average values of the activity coefficients as the activity coefficients of the counterions near the fixed ions inside the hydrogel, using the mean polymer

concentration calculated from the gel's swelling ratio (Q) and the mean activity obtained from MET measurements. Since the gel swells isotropically, the cube of the ratio of the thickness of the gel after phase separated DN gelation and swelling to the thickness of the poly(NaAMPS)gel immediately after preparation was used as the swelling ratio of the gel (Q).

$$Q = \left(\frac{t_{DN\,,sw}}{t_{1st,as-pre}} \right)^3 \quad (3)$$

$$\overline{C_{sw}} = \frac{C_{ini}}{Q} \quad (4)$$

$$\overline{\gamma_g} = \frac{\overline{a_g}}{\overline{C_{sw}}} \quad (5)$$

Here, $t_{DN\,,sw}$ is the thickness of the phase separated DN gel after swelling, and $t_{1st,as-pre}$ is the thickness of the poly(NaAMPS) gel before swelling in DMAAm solution. Since the charge of the PDMAAm gel, which is a neutral gel, has no effect on the Donnan potential measurement, the swelling ratio Q is the volume ratio of the poly(NaAMPS) gel. In addition, because the gel swells isotropically, the cube of the thickness change of the gel was used as the swelling ratio (Q). C_{ini} is the prepared monomer concentration. $\overline{C_{sw}}$, $\overline{a_g}$, and $\overline{\gamma_g}$ denote the average of the polymer concentration, the activity, and the activity coefficient, respectively.

$$C_g \simeq \frac{a_g}{\overline{\gamma_g}} \quad (6)$$

Assuming that the $\overline{\gamma_g}$ is equal to γ_g, the counterion concentration C_g for a fixed charge of the electrolyte polymer chain can be calculated using equation (6), using the concentration of mobile counterions around the local polyelectrolyte chains (a_g) obtained from the potential measurement. This result means that it is possible to estimate the polymer concentration from the Donnan potential, the preparation concentration of NaAMPS monomer and the swelling ratio in this experimental system.

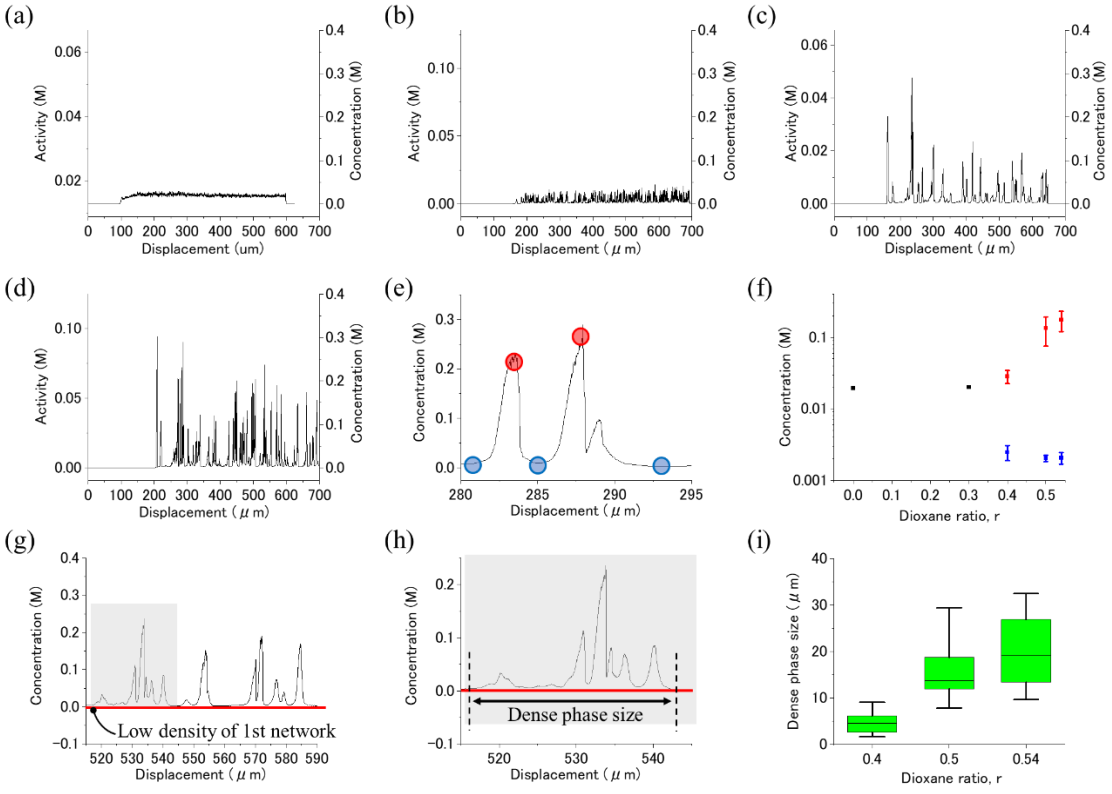

Figure 5. Concentration profiles and dense phase size of separated DN gels obtained from MET measurements. (a,b,c,d) Polymer concentration profiles of phase separation DN gels. We converted the phase separated DN gels' potentials obtained by MET into polymer concentration. Vertical axes: activity (M, left axis) or polymer concentration (M, right axis), horizontal axis: displacement (μm). Dioxane weight fractions r to precursor solution: (a) 0, (b) 0.4, (c) 0.5, (d) 0.54. (e) Polymer concentration of dense and sparse phases in the phase separated DN gel at r =0.54. Red and blue points are maximum and minimum concentrations, respectively. (f) The polymer concentration in the dense phase (red) and the mean polymer concentration in the sparse phase (blue) as a function of dioxane weight fraction. (g) Relationship between potential profile and dense phase size. The red line is the baseline of the sparse phase's polymer concentration. (h) Definition of the size of the dense phase based on the sparse phase's polymer concentration the part where the polyelectrolyte network is sparse). r = 0.54 is shown as an example. (i) Dense phase size in phase separated DN gels. The box plots for the 25th-75th percentiles were shown with the dense phase size on the vertical axis and the dioxane weight fraction (r) on the horizontal axis. Here, the whiskers indicate the 10th-90th percentile interval, and the straight line in the box represents the median. The sparse phase's polymer concentration for each concentration profile was 2.4×10^{-3} M at r = 0.4, 2.0×10^{-4} M at r = 0.5, and 2.1×10^{-4} M at r = 0.54.

Figure 5(a) showed the potential profiles as a function of displacement for r = 0, which is the reference in pure water, and r = 0.4, 0.5, and 0.54, where phase separation was confirmed and converted to activity and polymer concentration according to equation (2). The activity coefficient of the counterions inside the hydrogel (denoted as the activity coefficient of the hydrogel), $\overline{\gamma_g}$, was calculated using the average of the polymer concentration ($\overline{C_{sw}}$) derived by the swelling ratio of the gel and the average of the activity ($\overline{a_g}$) obtained from MET measurements according to equation (5). (Table 1)

Table 1.

Dioxane ratio r	Swelling ratio Q	Average polymer concentration $\overline{C_{sw}}$	Average activity $\overline{a_g}$	Average activity coefficient $\overline{\gamma_g}$
0	50	2.0×10^{-2} M	3.4×10^{-3} M	0.17
0.4	101	1.0×10^{-2} M	3.2×10^{-3} M	0.32
0.5	60	1.7×10^{-2} M	2.8×10^{-3} M	0.16
0.54	40	2.5×10^{-2} M	7.8×10^{-3} M	0.31

The PNaAMPS/PDMAAm DN gel with dioxane weight fraction r = 0 showed no internal phase separated structure. The obtained $\overline{\gamma_g}$ was 0.17, which is reasonable because it is close to the activity coefficient $\overline{\gamma_g}$ of 0.22 for the DN gel of PAMPS/PAAm in the study by Nakajima et al.[31] The $\overline{\gamma_g}$ values at r = 0.4, 0.5, and 0.54 for gels with a phase separated structure are assumed to be different for the dense and sparse phases. The method to measure the activity coefficients in the phases with

different concentrations has not yet been established. Therefore, we used the mean hydrogel activity coefficient calculated by the same method to obtain the activity coefficient for r = 0. The value of the activity coefficient $\overline{\gamma_g}$ obtained by this method may differ from the actual activity coefficient and therefore the polymer concentrations of the converted dense and sparse phases may also differ from the actual concentrations. However, since the difference does not affect the trend of polymer concentration change due to the difference in dioxane weight fraction, it can be sufficiently considered the actual polymer concentration. We succeeded in measuring the polymer concentration distribution of the gel in the depth direction of the phase separated DN gel from these plots (Figure 5(a)-5(d)).

The mean polymer concentration at each dioxane weight fraction obtained from the concentration profile was shown in Figure 5(e)-5(f). The red dots in the figure represent the mean polymer concentration in the dense phase, the blue dots represent the mean polymer concentration in the sparse phase, and the black dots represent the mean polymer concentration in the gel without phase separation. The mean polymer concentration in the dense phase was 2.8×10^{-2} M at r = 0.4, 1.3×10^{-1} M at r = 0.5, and 1.8×10^{-1} M at r = 0.54, respectively. The mean polymer concentration in the sparse phase was 2.5×10^{-3} M at r = 0.4, 2.0×10^{-4} M at r = 0.5, and 2.1×10^{-4} M at r = 0.54, respectively. We see that as the dioxane weight fraction increases, the concentration of the dense phase increases, and the concentration of the sparse phase decreases. The concentration of the dense phase was found to be 85

times that of the sparse phase in the highest density region. This result is consistent with the trend observed by contrast shading in the TEM images, indicating that, in contrast to the conventional qualitative measurement method, MET can continuously and quantitatively measure the local polymer concentration in a phase separated gel.

According to the discussion by Guo et al. [16], the counterion concentration ($C^+,\ C_g$) in the sparse phase is approximately 2.0×10^{-3} M according to Figure 5(f), and the polymer concentration ($C_p^-,\ C_{sw}$) is also the same based on the electrical neutrality condition according to equation (7). Since the reference solution (C_s) concentration is 10^{-5} M, the co-ion concentration (C^-) is 5.0×10^{-8} M according to equation (8).

$$C^+ = C^- + C_p^- \quad (7)$$

$$C_s^2 = C^+C^- \quad (8)$$

Since the co-ion concentration is sufficiently low compared to the fixed ion concentration, the Debye length in the sparse phase is estimated to be equal to the Debye length in pure water at pH 6.5 (about 540 nm). Since the counterion concentration (C^+) in the dense phase is more than 2.8×10^{-2} M according to Figure 5(f), the co-ion concentration (C^-) is less than 3.6×10^{-9} M and can be ignored. Therefore, the Debye length of the dense phase is about 540 nm, similar to the Debye length of the sparse phase.

TEM observation revealed the formation of a sea-island structure. The dense phase's size is defined as the area where the concentration is higher than the base concentration, red line, based on the concentration of the sparse polyelectrolyte chains in each concentration profile, as shown in Figure 5(g)-5(h). The base concentration of the polymer in each concentration profile was 2.5×10^{-3} M at r = 0.4, 2.0×10^{-4} M at r = 0.5, and 2.1×10^{-4} M at r = 0.54, respectively.

The dense phase sizes obtained from each concentration profile were shown in Figure 5(i) as box plots. Here, the box represented the 25th-75th percentile, the whiskers represented the 10th-90th percentile interval, and the straight line in the box represented the median. The results showed that the dense phase size obtained from MET at r = 0.4 is about 5 μm, at r = 0.5 is about 14 μm, and at r = 0.54 is about 20 μm. Therefore, as the dioxane concentration increases, the dense phase size also increases.

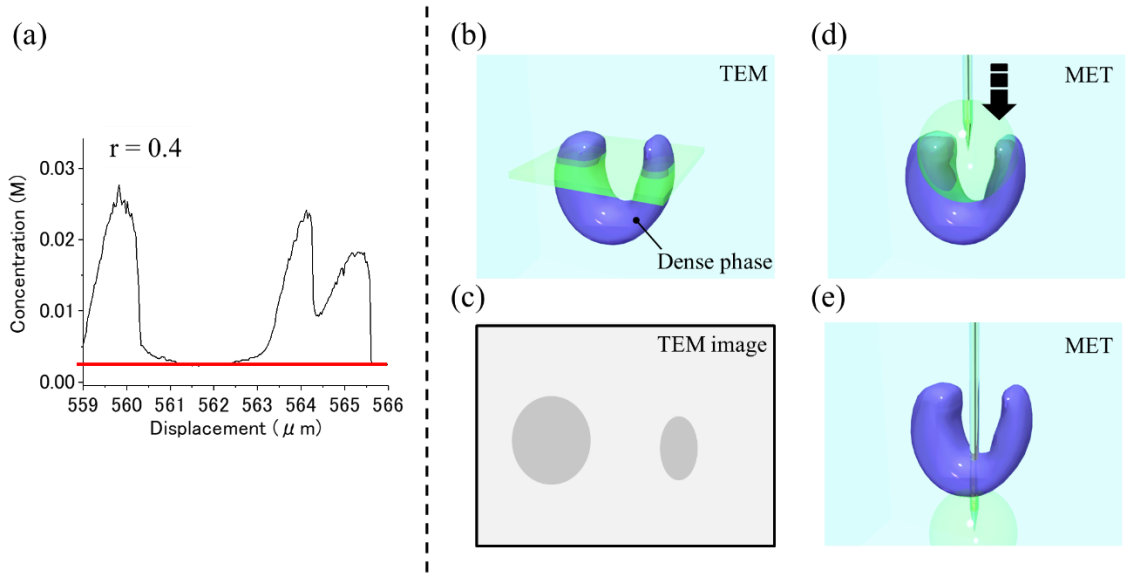

Figure 6. (a) The estimation of detection range and spatial resolution of MET. Characteristic peaks based on the concentration profile of the DN gel at r = 0.4. A partially enlarged view of the potential profile at a dioxane weight fraction of 0.4 is shown. The red line represents the base concentration. (b) The green rectangle shows the measurement cross-section of TEM. (c) The illustration shows a TEM image of the dense phase. (d)-(e) The green sphere shows the detection range of MET.

We considered the differences in the dense phase size as measured by TEM and MET. The corrected dense phase size obtained from the TEM image was 2.4±0.7 μm at r=0.4, and 5.2±1.2 μm at r = 0.54. respectively. In contrast, the dense phase size obtained from MET was about 5.0±2.8 μm at r = 0.4 and 20±8.6 μm at r = 0.54. Thus, the size of the dense phase obtained by MET is several times larger than that obtained from the TEM image. To understand why the dense phase size observed by

MET and TEM is different, we need to know the detection range and spatial resolution of MET. Figure 6(a) shows a magnified view of the potential profile at r = 0.4, where the concentration peak of the dense phase appears at 560 μm in displacement, then returns to the concentration band of the bulk gel, and then a new concentration peak of the dense phase appears at 564 μm. Therefore, the maximum detection range of MET is obtained by subtracting the length of the reference concentration region between the two concentration peaks from the length between the two concentration peaks. In this experiment, the detection range was determined to be less than 1.5 μm. As described above, if the concentration change is more than 2% in this experimental system, it can distinguish the concentration measurement from white noise. Therefore, it can be concluded that the concentration changes significantly exceeding the noise can be divided into two peaks in the 564-566 μm part of Figure 6(a). The distance between these two peaks is about 0.8 μm. Therefore, it should be noticed that the spatial resolution of MET is smaller than 0.8 μm (sub μm scale).

Based on this assumption, we consider why the dense phase size in MET is larger than that in TEM. The TEM sample is a thin layer section with a thickness of 100 nm thickness, but due to the cutting process all depth information is lost. For example, if the dense phase is present, as shown in Figure 6 (b)-(c), it is impossible to know if the size represents the maximum width of the dense phase or just some portion of the total phase. In contrast, the MET detection range is considered to be the range

where the KCl solution leaks from the tip of the glass electrode, which means that the detection range is spatially extended, as shown in Figure 6 (d)-(e). Besides, since the glass electrode is advanced at a constant speed, the MET can scan from the top of the dense phase to the bottom. However, because of its high sensitivity, the MET recognizes both the entrance into, as well as the exit out of the dense phase. Therefore, the observed dense phase size may be expressed as the total size of the diameter of the detection range and the original size of the dense phase. When the distance between one dense phase and the next dense phase on the measurement line is less than the size of the detection range of the MET, it is difficult to distinguish whether the obtained signal is one dense phase with different parts of concentration inside or multiple dense phases with different concentrations. Based on this analysis, MET provides us with a method to more accurately measure the local size and shape of phase separated hydrogels.

Conclusion

Through improvements to our microelectrode system we were able to reduce the electrical noise during measurement, making it possible to measure concentration changes of 1.02×10^{-5} M (2%) from the noise when the reference solution is 10^{-5} M. We succeeded in measuring the size of dense and sparse phases as well as observing the spatial distribution of these phases in a hydrogel by using the microelectrode technique (MET). Furthermore, by using MET, we succeed in quantitatively

measuring the local concentration inside the electrolyte hydrogel, which is impossible with other conventional measurement methods. The mean activity coefficients of the counterions in electrolyte hydrogels can be measured quantitatively. Therefore, we can say that MET is an innovative new measurement method that can locally and quantitatively measure the concentration distribution of structures inside hydrogels. In addition, the MET concentration profile shows the existence of sub-μm scale structures in the phase separated DN gels. We estimate that the MET detection range is less than 1.5 μm and the spatial resolution is less than 0.8 μm. Therefore, MET enables us to measure the concentration distribution of microphase separated polyelectrolyte structures with very high resolution. The average activity coefficients are successfully estimated from the average values of the activity in the activity profiles for each dioxane ratio obtained using MET and the swelling degree of the hydrogel. We find that the polymer concentration in the phase separated dense phase is up to 85 times higher than in the sparse phase. This technique is effortless to prepare for measurement and allows for in-situ potential measurements. It is also applicable to biomaterials consisting of charge-containing components such as various types of cells and living tissues. Therefore, this method is expected to be used not only for measuring the concentration distribution of polyelectrolyte hydrogels but also as a criterion for in vivo pathology determination, for example, to identify the distribution of aggregate formation (amyloid-β, etc.) in organs and tissues in-situ by measuring the structure and concentration changes in vivo.

Supporting information

Thickness of the hydrogels, swelling ratio of phase separated DN gels, schematic image of DN gel.

Acknowledgements

We would like to thank Dr. Masakazu Takahata for his technical guidance and Daniel R. King for his helpful comments. This research was financially supported by JSPS KAKENHI Grant numbers JP17H06144. We also acknowledge the Open Facilities of Hokkaido University Sousei Hall, for TEM sample preparation. J.P.G. acknowledges the Institute for Chemical Reaction Design and Discovery established by World Premier International Research Initiative, Ministry of Education, Culture, Sports, Science and Technology (MEXT), Japan.

References

(1) Jian Ping Gong; Kurokawa, T.; Narita, T.; Kagata, G.; Osada, Y.; Nishimura, G.; Kinjo, M. Synthesis of Hydrogels with Extremely Low Surface Friction [4]. *Journal of the American Chemical Society*. **2001**, pp 5582–5583. https://doi.org/10.1021/ja003794q.

(2) Azuma, C.; Yasuda, K.; Tanabe, Y.; Taniguro, H.; Kanaya, F.; Nakayama, A.; Yong, M. C.; Jian, P. G.; Osada, Y. Biodegradation of High-Toughness Double Network Hydrogels as

Potential Materials for Artificial Cartilage. *Journal of Biomedical Materials Research - Part A* **2007**, *81* (2), 373–380. https://doi.org/10.1002/jbm.a.31043.

(3) Yasuda, K.; Gong, J. P.; Katsuyama, Y.; Nakayama, A.; Tanabe, Y.; Kondo, E.; Ueno, M.; Osada, Y. Biomechanical Properties of High-Toughness Double Network Hydrogels. *Biomaterials* **2005**, *26* (21), 4468–4475. https://doi.org/10.1016/j.biomaterials.2004.11.021.

(4) Gong, J. P.; Katsuyama, Y.; Kurokawa, T.; Osada, Y. Double-Network Hydrogels with Extremely High Mechanical Strength. *Advanced Materials* **2003**, *15* (14), 1155–1158. https://doi.org/10.1002/adma.200304907.

(5) Sun, T. L.; Kurokawa, T.; Kuroda, S.; Ihsan, A. bin; Akasaki, T.; Sato, K.; Haque, M. A.; Nakajima, T.; Gong, J. P. Physical Hydrogels Composed of Polyampholytes Demonstrate High Toughness and Viscoelasticity. *Nature Materials* **2013**, *12* (10), 932–937. https://doi.org/10.1038/nmat3713.

(6) Nonoyama, T.; Lee, Y. W.; Ota, K.; Fujioka, K.; Hong, W.; Gong, J. P. Instant Thermal Switching from Soft Hydrogel to Rigid Plastics Inspired by Thermophile Proteins. *Advanced Materials* **2020**, *32* (4). https://doi.org/10.1002/adma.201905878.

(7) Pataky, K.; Braschler, T.; Negro, A.; Renaud, P.; Lutolf, M. P.; Brugger, J. Microdrop Printing of Hydrogel Bioinks into 3D Tissue-like Geometries. *Advanced Materials* **2012**, *24* (3), 391–396. https://doi.org/10.1002/adma.201102800.

(8) Sultan, S.; Mathew, A. P. 3D Printed Scaffolds with Gradient Porosity Based on a Cellulose Nanocrystal Hydrogel. *Nanoscale* **2018**, *10* (9), 4421–4431. https://doi.org/10.1039/c7nr08966j.

(9) Bendtsen, S. T.; Quinnell, S. P.; Wei, M. Development of a Novel Alginate-Polyvinyl Alcohol-Hydroxyapatite Hydrogel for 3D Bioprinting Bone Tissue Engineered Scaffolds. *Journal of Biomedical Materials Research - Part A* **2017**, *105* (5), 1457–1468. https://doi.org/10.1002/jbm.a.36036.

(10) Odent, J.; Vanderstappen, S.; Toncheva, A.; Pichon, E.; Wallin, T. J.; Wang, K.; Shepherd, R. F.; Dubois, P.; Raquez, J. M. Hierarchical Chemomechanical Encoding of Multi-Responsive Hydrogel Actuators: Via 3D Printing. *Journal of Materials Chemistry A* **2019**, *7* (25), 15395–15403. https://doi.org/10.1039/c9ta03547h.

(11) Zolfagharian, A.; Kouzani, A. Z.; Khoo, S. Y.; Nasri-Nasrabadi, B.; Kaynak, A. Development and Analysis of a 3D Printed Hydrogel Soft Actuator. *Sensors and Actuators, A: Physical* **2017**, *265*, 94–101. https://doi.org/10.1016/j.sna.2017.08.038.

(12) Matsunaga, T.; Shibayama, M. Gel Point Determination of Gelatin Hydrogels by Dynamic Light Scattering and Rheological Measurements. *Physical Review E - Statistical, Nonlinear, and Soft Matter Physics* **2007**, *76* (3). https://doi.org/10.1103/PhysRevE.76.030401.

(13) Hurukawa, H.; Okada, M. Scanning Microscopic Light Scattering of Inhomogeneous Polyacrylamide Gel. *Trans. Mater. Res. Soc. Jpn* **2000**, *25(3)*.

(14) Tominaga, T.; Tirumala, V. R.; Lin, E. K.; Gong, J. P.; Furukawa, H.; Osada, Y.; Wu, W. li. The Molecular Origin of Enhanced Toughness in Double-Network Hydrogels: A Neutron Scattering Study. *Polymer* **2007**, *48* (26), 7449–7454. https://doi.org/10.1016/j.polymer.2007.10.016.

(15) Tanaka, W.; Shigemitsu, H.; Fujisaku, T.; Kubota, R.; Minami, S.; Urayama, K.; Hamachi, I. Post-Assembly Fabrication of a Functional Multicomponent Supramolecular Hydrogel Based on a Self-Sorting Double Network. *Journal of the American Chemical Society* **2019**, *141* (12), 4997–5004. https://doi.org/10.1021/jacs.9b00715.

(16) Cascone, M. G.; Lazzeri, L.; Sparvoli, E.; Scatena, M.; Serino, L. P.; Danti, S. Morphological Evaluation of Bioartificial Hydrogels as Potential Tissue Engineering Scaffolds. *Journal of Materials Science: Materials in Medicine* **2004**, *15* (12), 1309–1313. https://doi.org/10.1007/s10856-004-5739-z.

(17) Suzuki, A.; Yamazaki, M.; Kobiki, Y.; Suzuki, H. Surface Domains and Roughness of Polymer Gels Observed by Atomic Force Microscopy. *Macromolecules* **1997**, 30 (8), 2350-2354. https://doi.org/10.1021/ma961598r

(18) L Hodgkin, B. A.; Katz, B.; Biological Association, M. The Effect of Sodium Ions on The Electrical Activity of The Giant Axon of The Squid. *The journal of Physiology* **1949**, 108 (1), 37-77. 10.1113/jphysiol.1949.sp004310

(19) Lee, C. W.; Szymanska, A. A.; Ikegaya, Y.; Nenadic, Z. The Accuracy and Precision of Signal Source Localization with Tetrodes. In *Proceedings of the Annual International Conference of the IEEE Engineering in Medicine and Biology Society, EMBS*; **2013**; pp 531–534. https://doi.org/10.1109/EMBC.2013.6609554.

(20) Takahata, T.; Hayashi, M.; Ishikawa, T. SK4/IK1-like Channels Mediate TEA-Insensitive, Ca 2-Activated K Currents in Bovine Parotid Acinar Cells. *Am J Physiol Cell Physiol* **2003**, *284*, 127–144. https://doi.org/10.1152/ajpcell.00250.2002.-Although.

(21) Aonuma, H.; Nagayama, T.; Takahata, M. *Distribution of Autofluorescent Cell Bodies in the Crayfish Central Nervous System*; **1996**.

(22) Purves, R. D. Microelectrode Methods for Intracellular Recording and Iontophoresis. *Academic Press: London*, **1981**, 33.

(23) Elliott, G. F.; Bartels, E. M. Donnan Potential Measurements in Extended Hexagonal Polyelectrolyte Gels Such as Muscle. *Biophysical Journal* **1982**, *38* (2), 195–199. https://doi.org/10.1016/S0006-3495(82)84546-3.

(24) Guo, H.; Kurokawa, T.; Takahata, M.; Hong, W.; Katsuyama, Y.; Luo, F.; Ahmed, J.; Nakajima, T.; Nonoyama, T.; Gong, J. P. Quantitative Observation of Electric Potential Distribution of Brittle Polyelectrolyte Hydrogels Using Microelectrode Technique. *Macromolecules* **2016**, *49* (8), 3100–3108. https://doi.org/10.1021/acs.macromol.6b00037.

(25) Blyakhman, F. A.; Safronov, A. P.; Zubarev, A. Y.; Shklyar, T. F.; Dinislamova, O. A.; Lopez-Lopez, M. T. Mechanoelectrical Transduction in the Hydrogel-Based Biomimetic Sensors. *Sensors and Actuators, A: Physical* **2016**, *248*, 54–61. https://doi.org/10.1016/j.sna.2016.06.020.

(26) Safronov, A.P.; Kamalov, I.A.; Shklyar, T.F.; Dinislamova, O.A.; Blyakhman, F.A. Activity of Counterions in Hydrogels Based on Poly(acrylic acid) and Poly(methacrylic acid): Potentiometric Measurements. *POLYMER SCIENCE Ser. A* **2012**, , 54 (11), 909–919.

(27) Guo, H.; Hong, W.; Kurokawa, T.; Matsuda, T.; Wu, Z. L.; Nakajima, T.; Takahata, M.; Sun, T.; Rao, P.; Gong, J. P. Internal Damage Evolution in Double-Network Hydrogels Studied by Microelectrode Technique. *Macromolecules* **2019**, *52* (18), 7114–7122. https://doi.org/10.1021/acs.macromol.9b01308.

(28) Donnan, F. G. Theory of Membrane Equilibria and Membrane Potentials in the Presence of Non-Dialysing Electrolytes. A Contribution to *Physical-Chemical Physiology*; **1995**; Vol. 100.

(29) Kawauchi, Y.; Tanaka, Y.; Furukawa, H.; Kurokawa, T.; Nakajima, T.; Osada, Y.; Ping Gong, J. Brittle, Ductile, Paste-like Behaviors and Distinct Necking of Double Network Gels with Enhanced Heterogeneity. In *Journal of Physics: Conference Series*; Institute of Physics Publishing, **2009**; Vol. 184. https://doi.org/10.1088/1742-6596/184/1/012016.

(30) Kiyama, R.; Nonoyama, T.; Sedlacik, T; Jinnai H; Gong, J. P. Single-Macromolecular Level Imaging of a Hydrogel Structure. *ChemRxiv* **2021**. https://doi.org/10.33774/chemrxiv-2021-x1s5k

(31) Nakajima, T.; Chida, T.; Mito, K.; Kurokawa, T.; Gong, J. P. Double-Network Gels as Polyelectrolyte Gels with Salt-Insensitive Swelling Properties. *Soft Matter* **2020**, *16* (23), 5487–5496. https://doi.org/10.1039/d0sm00605j.